

Interpretation of gas chimney from seismic data using artificial neural network: A study from Maari 3D prospect in the Taranaki basin, New Zealand



Deepak Singh, Priyadarshi Chinmoy Kumar, Kalachand Sain*

CSIR-National Geophysical Research Institute, Uppal Road, Hyderabad, India

ARTICLE INFO

Article history:

Received 1 June 2016

Received in revised form

11 October 2016

Accepted 22 October 2016

Available online 24 October 2016

Keywords:

Seismic attributes

Neural network

3D visualization

Gas chimney

Interpretation

ABSTRACT

The seismic interpretation in Maari 3D prospect of the Taranaki basin in New Zealand based on artificial neural network has brought out gas migration pathways from the source rock through the faulted reservoirs to the seabed. The findings correlate reasonably with the results of Moki-1 well drilled within the study region. The gas chimneys are analyzed using modern 3D visualization tools by displaying the chimney probability cube over different vertical seismic sections, horizon slices and time slices respectively. The training of multi-seismic attributes resulted into 0.4–0.6 normalized RMS error giving rise to 5.08–10.26% misclassification during the training and testing phases. Several fault intersection zones (weak zones) within the reservoirs exhibit high probability of gas chimneys. This study acts as an add-on-tool for understanding the petroleum system and provides preventive clues for mitigating hazards in future exploitation program.

© 2016 Published by Elsevier B.V.

1. Introduction

Gas chimneys are form of chaotic disordered vertical disturbances observed on seismic data, where the reflectors are discontinuous and reflection amplitudes are weaker. Mapping chaotic reflections from seismic data and gleaming valuable information for exploration of hydrocarbons is a challenge. Dunbar et al. (1998) used a phase based velocity modeling approach for imaging gas clouds. O'Brien et al. (1999) used a detailed velocity modeling approach for simulating the effect of gas chimney. Engelhardt et al. (2001) made use of four component seismic data for interpreting gas chimneys. During the past 20 years, seismic interpretation has witnessed significant development of new seismic attributes and their application for imaging and interpreting geological features of interest (Bahorich and Farmer, 1995; Hardage et al., 1996; Marfurt et al., 1998, 1999; Tingdahl, 1999; Tingdahl et al., 2001; Roberts, 2001; Tingdahl and de Rooij, 2005; Al-Dossary and Marfurt, 2006; Chopra and Marfurt, 2007; Chen et al., 2008; Farfour et al.,

2015). The use of advanced interpretation techniques based on different seismic attributes such as similarity, energy, dip variance, frequency etc., are very sensitive in illuminating the chaotic events from the surroundings (Brouwer et al., 2008; Connolly and Garcia, 2012). They are commonly supplemented with low similarity, low amplitude, variable dip wipe-out zone, causing high frequency attenuation due to scattering of seismic signals (Berndt et al., 2003; Ligtenberg, 2003; Westbrook et al., 2008; Brouwer et al., 2008; Petersen et al., 2010; Connolly and Garcia, 2012).

The identification of gas chimneys provides a clue for the existence of hydrocarbons and helps in understanding the petroleum system of a region. This also identifies potential over-pressured zones in mitigating the drilling risks (Heggland, 2004). However, some authors (Heggland, 1997; Aminzadeh et al., 2002; Connolly and Garcia, 2012) refer these events as an effective source of noise that degrades the quality of seismic image. Hence, it has been a challenge for effective identification and mapping of causative bodies that may lead to the exploration of hydrocarbons. It is the seismic attributes that can assuage such challenge. The attributes such as the root mean square, variance and red-green-blue color blending are mostly used to study and interpret these chaotic events. However, seismic interpreters encounter problems in extracting seismic attributes for outlining the objects of interests, as

* Corresponding author.

E-mail addresses: negi.ds@yahoo.com (D. Singh), kalachandsain@yahoo.com (K. Sain).

the attributes sometimes cannot discriminate the objects associated with different origin. To alleviate such discrepancies, Meldahl et al. (1999) proposed a technique that draws a proper definition of the targeted feature. The approach is based on computation of several multi-trace attributes and recombination of extracted attributes into one or two new attributes through artificial neural network (NN). The present work for the delineation of gas chimneys over the Maari field of southern Taranaki basin, offshore New Zealand, is focused on this philosophy.

Ilg et al. (2012) have identified ~394 gas chimneys within the Taranaki basin (Fig. 1) based on seismic attribute studies. These features are found to be more concentrated within the offshore southern Taranaki basin. Later, Alotaibi (2015) and Wooltorton (2015) illustrates the gas chimneys within the Maari prospect, which are related to faults. These works are based on the root mean square, variance and red-green-blue color blending techniques. Using one or two attributes for interpreting chaotic events that represents hydrocarbon (gas) shows may be debatable. In this study, we use a combination of directive multi-trace attributes (i.e., attributes steered in a user driven or data driven direction) to generate a new attribute through supervised NN. The attributes that have been used here are similarity, energy, dip variance and frequency wash-out that can enhance the contrast between the chaotic events and the background in a robust way. Before training the network, the attributes are extracted from the dip-steered seismic data which is prepared from a steering cube that stores the dip and azimuth information at every sample position of seismic reflectors. This forms the heart of the entire work flow. It is to be mentioned that multiple vertical windows are used while extracting the attributes. The training is then performed on these

extracted attributes at every chimney and non-chimney locations chosen on seismic data by the interpreter using a fully connected multi-layer perceptron (MLP) NN. Once the training is found suitable based on RMS error between the observation and the prediction, it is applied over the entire seismic data set to classify them into chimney (high-probability) and non-chimney (low-probability) zones, resulting into a 3D probability chimney volume or chimney cube. The output are then validated with several key parameters that not only infers the presence of gas chimneys but also helps in understanding the petroleum system of the region.

2. Geology and tectonics

The Taranaki basin (TB) (Fig. 1) is the only sedimentary basin of New Zealand, which is known for its enormous hydrocarbon potential (Palmer and Andrews, 1993; King and Thrasher, 1996) with complex subsurface geology. It covers an approximate area of 100,000 km² (King and Thrasher, 1996), and is located along the western coast of North Island, New Zealand and lies over the subduction zone between the Pacific Plate and the Australian Plate. The basin is a store house for a thick pile (up to 9 km) of sedimentary sequences of the Cretaceous to Recent time (Reilly et al., 2015). The eastern part of the basin is bounded by the subsurface Taranaki Fault and the Patea-Tongaporutu High (Fig. 2) and covered by the Late Miocene and Pliocene sediments. Kamp et al. (2004) documented that these sediments possess a lateral continuity with sediments of the south Wanganui basin. Most of the sedimentary deposits belong to the southern part of the basin that includes the famous Maari, Maui and Tui fields. It is reported that these fields contribute almost 70% of annual oil production (~180 million barrel of oil equivalent). The western part of the basin imparts its extension beyond the present day continental shelf thereby merging with the Northland basin to the north (King and Thrasher, 1996). However, the northern and southern borders of the basin are poorly outlined.

The TB comprises of two major structural units i.e. the Western Stable Platform and the Eastern Mobile Belt (Fig. 2). The Western Stable Platform did not witness any tectonic activity and continued to remain relatively quiescent since the Cretaceous (King and Thrasher, 1996; Higgs et al., 2012). King and Thrasher (1996) and Higgs et al. (2012) have outlined this stable platform as a progradational depositional sequence on an unfaulted, sub-horizontal regionally subsiding sea floor. However, the Eastern Mobile Belt exhibits a complex geological morphology representing heavy tectonism leading to the Neogene development. The Cretaceous-Cenozoic succession of the basin consists of terrestrial, marine sedimentary and volcanic deposits which lie over the basement of the Paleozoic-Mesozoic granites, basalts, andesite and meta-sediments (Fig. 3) (King and Thrasher, 1996; Hart, 2001). The basin evolved during the Late Cretaceous extensional faulting that was associated with the breakup of Gondwana and formation of the Tasman Sea and fault bounded grabens and half graben structures. These structural features were filled by synrift sedimentary deposits comprising of interbedded coal measures and sandstone sequences that have resulted into the formation of the Pakawau Group (Fig. 3) (Palmer and Andrews, 1993; King and Thrasher, 1996). Thereafter, the basin underwent a major transgressive phase overlying the Paleocene and Eocene deposits of post-rift and late-rift transgressive sedimentary sequences. This transgressive event over the entire region led to the deposition of terrestrial to marginal marine sequences of the Kapuni Group (Farewell, Kaimiro, Mangahewa and McKee Formations). Inactive tectonism and reduction in clastic sediment supply during the Oligocene period formed widespread deposition of limestones and calcareous mudstones of the Ngatoro Group (Otaraoa and Tikorangi

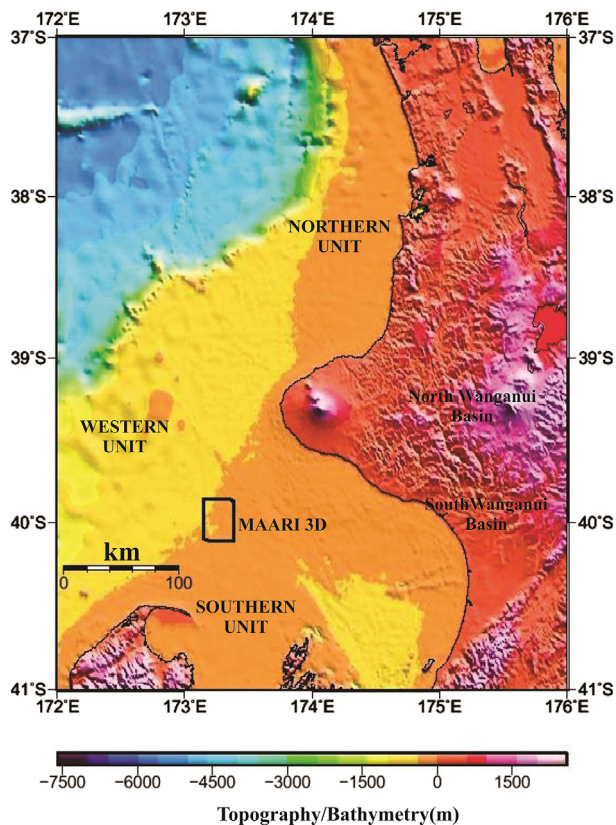


Fig. 1. Location of the study area, covering an area of 123.20 km² in the southern part of the Taranaki basin. The Maari 3D seismic block is marked by a black square.

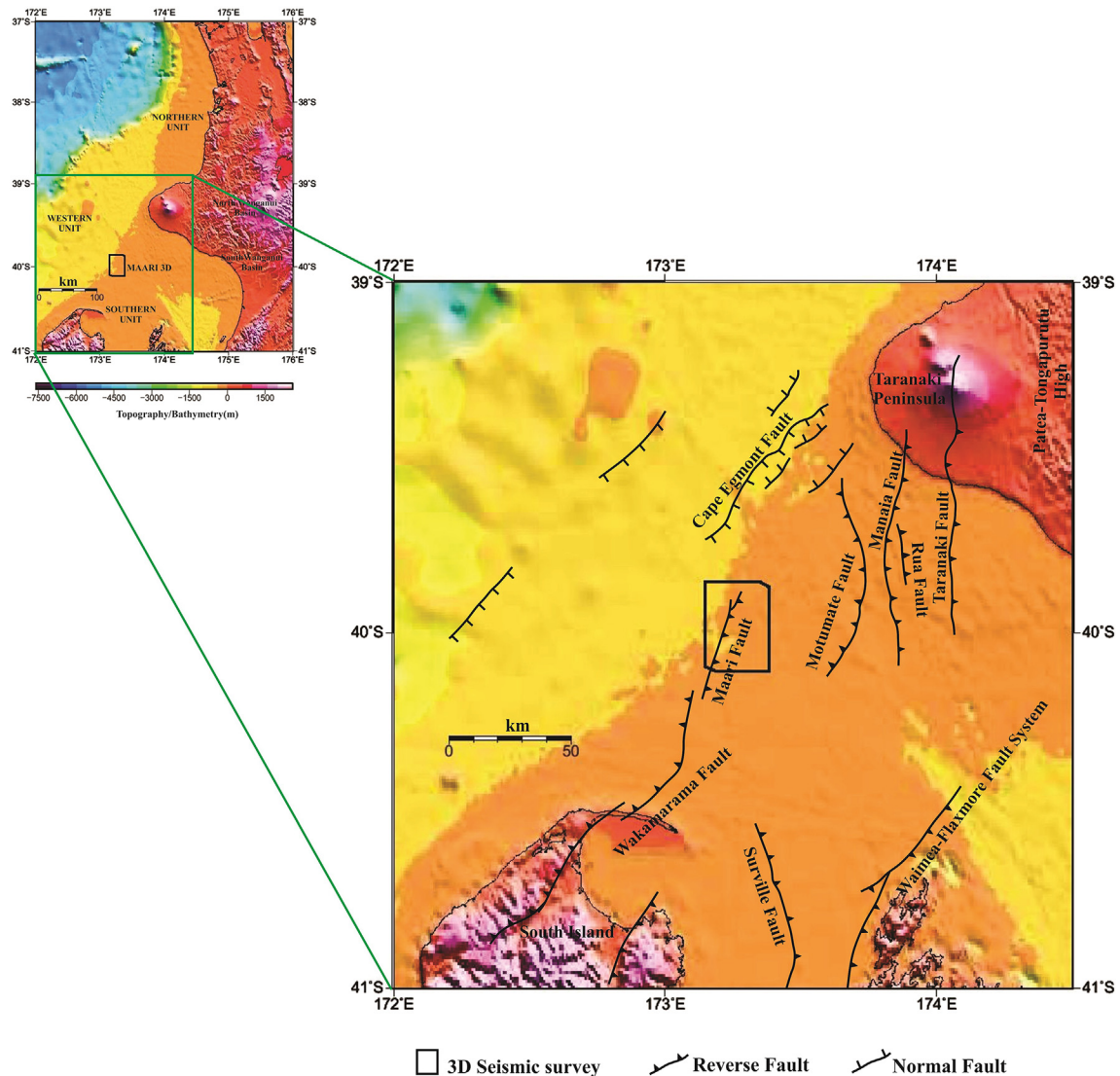


Fig. 2. Tectonic Map of the Taranaki basin overlain with topography-bathymetry map showing several tectonic elements (normal and reverse faults). The Maari 3D seismic block indicated by a black square is cut by reverse faults (Modified after Reilly et al., 2015).

Formations) throughout the basin (King et al., 1999; King, 2000). Transgressive phase reached to its climax in the early Miocene (Ngatoro Group: Taimana Formation and Wai-iti Group: Manganui Formation) and regressive phase started from the Mid-Miocene comprising of the Wai-iti Group (Moki, Mohakatino Formations) through the Pliocene (Rotokare Group) to the present day situation. The important hydrocarbon source rock intervals include the Cretaceous synrift terrestrial coaly facies, the Paleocene organic-rich marine mudstone and the Eocene terrestrial/estuarine coaly sequence (King and Thrasher, 1996; Hart, 2001). The Cretaceous-Paleogene rifting phase and the late Miocene reactivation developed many potential structural traps within the basin. These subsurface structural features contribute to the trapping mechanism within the basin and contains largest accumulation of hydrocarbon deposits.

3. The data

This study is accomplished using 3D seismic survey of the Maari prospect which lies over the southern part of offshore Taranaki

Basin (Fig. 1). The seismic data, acquired in 1999 by the Geo-Prakla Company, is a 3D time migrated seismic volume covering an area of $\sim 123.20 \text{ km}^2$. The data were acquired in $25.00 \text{ m} \times 12.50 \text{ m}$ (inl/crl bin) with 4.0 m sampling interval and 72 foldage. The total record length of the data is 3.0 s, and the volume comprises 405 inlines (Line no. 460 to 865) and 970 crosslines (Line no. 1070 to 2040). The seismic data polarity is SEG normal i.e. the increase in acoustic impedance boundary is reflected as peak or positive amplitude. The prospect area has been drilled by 7 wells namely Kea-1, Maari-1A, Maari-2, Maui-4, Moki-1, Moki-2 and MR9P6.

4. Neural network and seismic attributes

4.1. Neural networks

The concept of artificial neural network (ANN) is inspired by the research of McCulloch and Pitts (1943) that tries to mimic the behavior of biological neuron (de Groot, 1999; Van der Baan and Jutten, 2000). The basic principle is to feed a weighted sum of inputs into an activation function which is non-linear in nature to

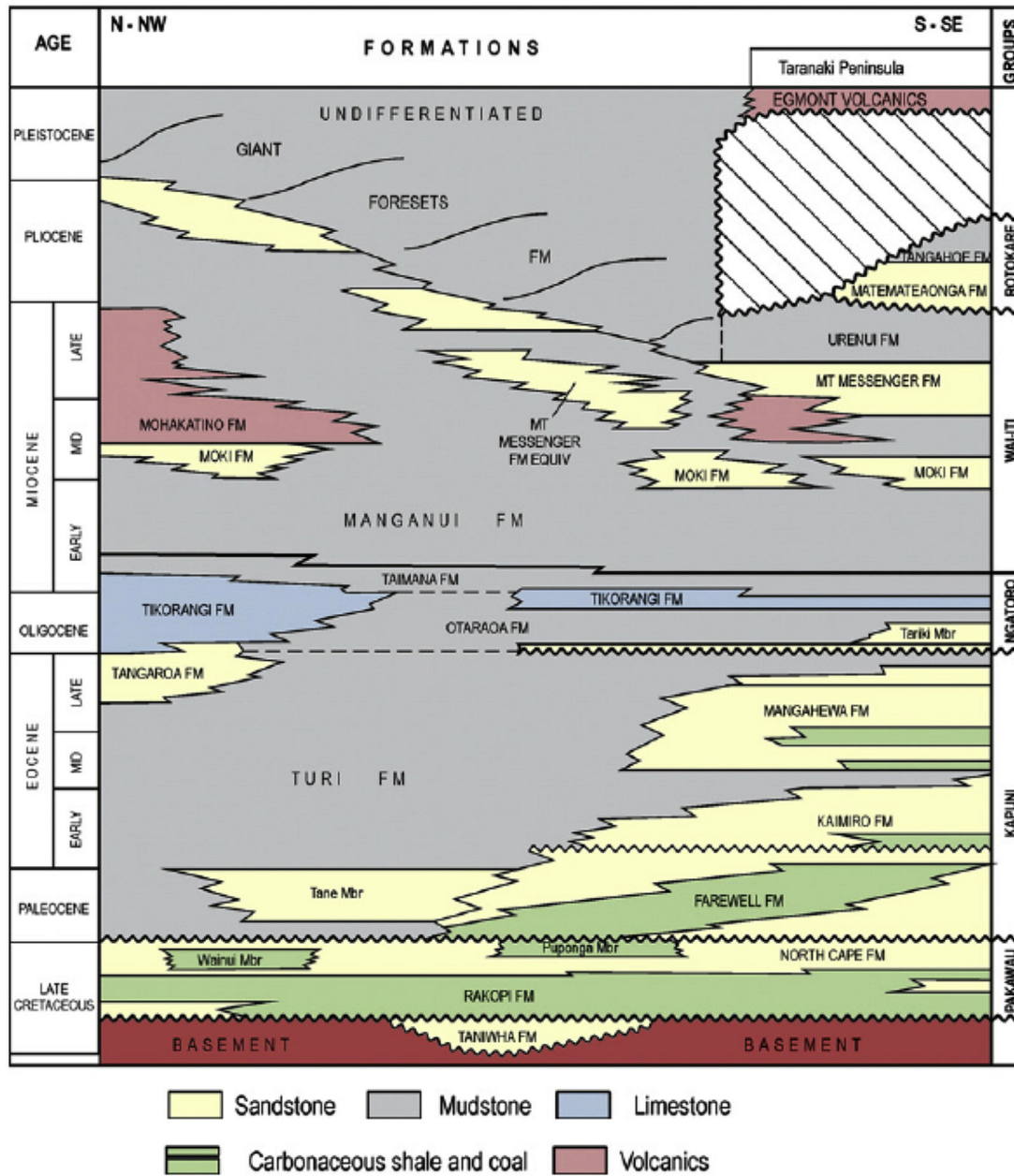


Fig. 3. Litho-stratigraphy map of the Taranaki basin (after, King and Thrasher, 1996).

rescale the sum. A constant bias (node or threshold) is applied to this process for maintaining and controlling the connection between the input and the processor for a decisional output, which is examined critically. The weight, assigned to each input unit, plays a pivotal role. The more the weight, the better is the connection between the input and the processor. If the response output is found to be different from the expected output, the internal parameters such as inputs and weights (known as synaptic weights) are rechecked and rescaled to establish a better match between the obtained and targeted outputs.

The present study follows a supervised learning mechanism - a technique in which the NN is trained on the data points selected by the interpreter in order to classify the training response into two or more classes (de Groot, 1995; Ligtenberg and Wansink, 2001; de Groot et al., 2004; Brouwer et al., 2011). This learning process is

carried out through a multi-layered perceptron (MLP) network (Rosenblatt, 1962), which consists of a large number of interconnected processing nodes, organized into input layer, hidden layer and output layer. The data fed into the MLP network moves from input layer through hidden layer to the output layer. Basically, the MLP works on two basic principles: abstraction and generalization (de Groot, 1995; Brouwer et al., 2011), where abstraction is the ability to extract the relevant features from the input and discard the irrelevant ones. Once trained, the generalization allows the network to recognize the input that are not part of the training set.

The training of the network is carried out with a random set of weights iteratively in such a way that connection weights are updated and problems such as the local minima are avoided (Atakulreka and Sutivong, 2007). The iterative training is continued

till a minimum error between the NN prediction and the actual or known is obtained. Once this is achieved, the network classifies the output into different classes. In the present analysis, the output is chimney-yes and chimney-no. The activation function used in our MLP network is the sigmoid function, which helps to rescale the neural output. This function is continuous, monotonically increasing, differentiable and bounded, and takes the input and squashes the output in terms of 0s and 1s. 0 refers to chimney-no or low chimney effect and 1 refers to chimney-yes or high chimney effect.

The MLP network is robust, can deal with large volume of input data and quickly extract relevant information from the data (de Groot, 1995). Such non-linear network has found important application in characterization of seismic reservoir, extraction of geologic features and recognition of patterns (An and Moon, 1993; Wong et al., 1995; Mohaghegh et al., 1996; Schuelke et al., 1997; de Groot, 1999; Ligtenberg and Wansink, 2001; Ligtenberg, 2005).

4.2. Seismic attributes

Seismic attributes are defined as the quantities measured, computed and inferred from the seismic data, and help in enhancing the geologic feature or quantifying reservoir property of interest (Chopra and Marfurt, 2007). A set of seismic attributes, which are useful inputs for training the neuron model, are described below.

4.2.1. Similarity

Similarity expresses how much two or more segments of seismic traces $u(x, y, t)$ look alike. If we consider the samples of trace segments to be the coordinates of vectors in hyperspace, the similarity is defined as the Euclidean distance between the vectors, normalized over the vector lengths (Tingdahl, 2003; Tingdahl and de Groot, 2003; Tingdahl and de Rooij, 2005). Thus, if S is the similarity between two trace segments at (x_A, y_A) and (x_B, y_B) , centered at time t , the Euclidean distance is expressed as:

$$S = 1 - \frac{|a - b|}{|a| + |b|} \tag{1}$$

where:

$$a = [u(x_A, y_A, t + t_1)u(x_A, y_A, t + t_1 + dt) \ u(x_A, y_A, t + t_2)u(x_A, y_A, t + t_2 - dt)]$$

$$b = [u(x_B, y_B, t + t_1)u(x_B, y_B, t + t_1 + dt) \ u(x_B, y_B, t + t_2)u(x_B, y_B, t + t_2 - dt)]$$

dt is the sampling interval, t_1 and t_2 are the relative start and stop times of the comparison window and u is the seismic amplitude.

The similarity outputs range between 0 and 1, where 0 represents low similarity and 1 represents high similarity. In the context of chimney analysis, seismic chimneys are associated with low similarity values.

When similarity attribute is computed from dip-steering seismic (Tingdahl, 2003), the output is called dip-steered similarity, which is expressed as (Tingdahl, 2003):

$$S_{dip} = 1 - \frac{|a_{dip} - b_{dip}|}{|a_{dip}| + |b_{dip}|} \tag{2}$$

where:

$$a_{dip} = [u(x_A, y_A, t_A + t_1)u(x_A, y_A, t_A + t_1 + dt) \ u(x_A, y_A, t_A + t_2) - dt)u(x_A, y_A, t_A + t_2)]$$

$$b_{dip} = [u(x_B, y_B, t_B + t_1)u(x_B, y_B, t_B + t_1 + dt) \ u(x_B, y_B, t_B + t_2 - dt)u(x_B, y_B, t_B + t_2)]$$

t_A and t_B are the dip-steered times from the position (x, y, t) to the traces at (x_A, y_A) and (x_B, y_B) respectively. The use of dip-steered similarity delivers an improved chimney classification from the background.

4.2.2. Energy

The Energy attribute at (x, y, t) is defined as the sum of the squared amplitudes within a given window (Tingdahl, 2003), and is given by:

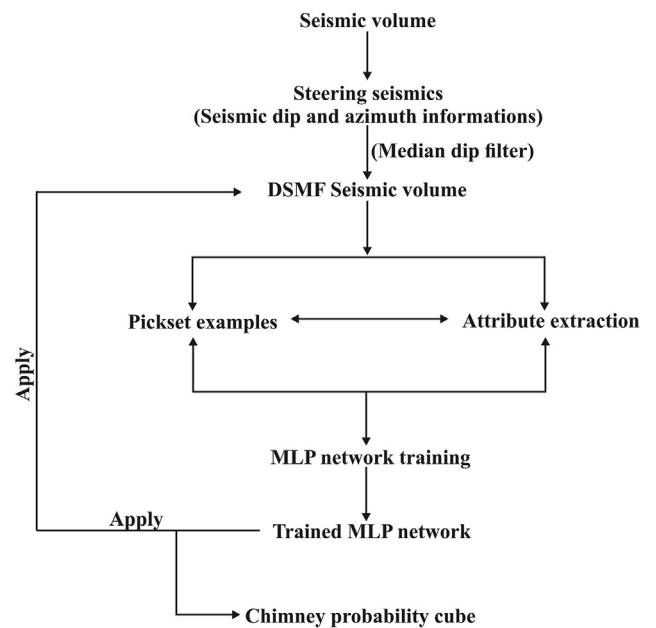
$$E = \sum_{\tau=t_1}^{t_2} u(x, y, t + \tau)^2 \tag{3}$$

where, t_1 and t_2 are the relative start and stop times of the energy window.

The chimneys are outlined as low amplitude and low energy disturbed events.

4.2.3. Dip variance

Seismic attribute that honors the directionality property (Tingdahl, 2003; Tingdahl and de Rooij, 2005) provides a better classification scheme to identify features of interpreter's interest. In the context of seismic chimneys, the inner parts of these features are outlined with chaotic textures. These zones are represented by variable dips i.e. the dips varying from sample to sample within these zones. These behaviors can be efficiently characterized by measuring statistical variance of dips as (Tingdahl, 2003):



DSMF : Dip steered median filter
MLP : Multi-layered Perceptron

Fig. 4. ANN Workflow used in the present study.

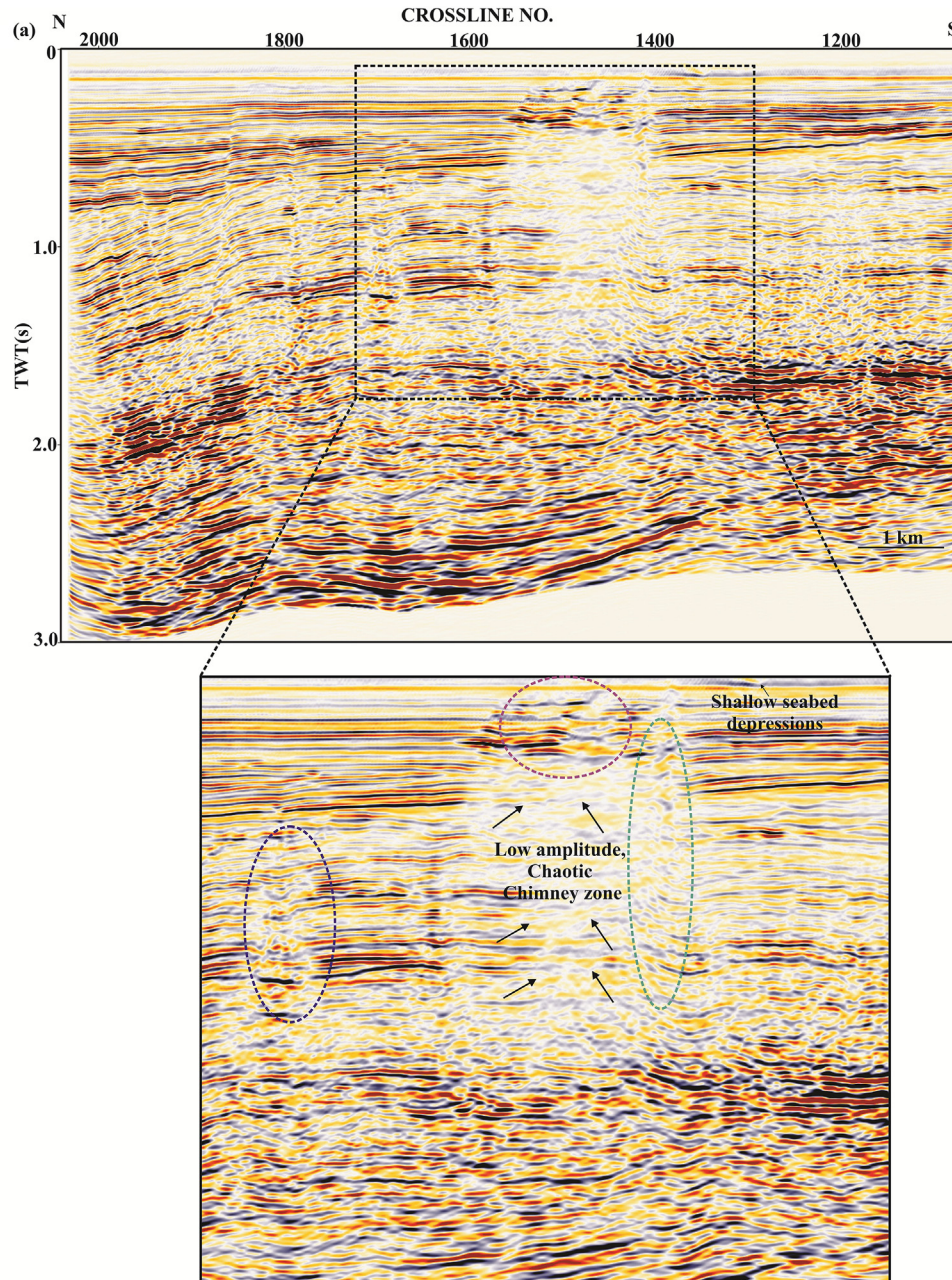


Fig. 5. a: Original pre-stack time migrated seismic section for inline no. 693 from Maari 3D seismic volume. The signals within the violet, green and pink ovals in the zoomed section are observed weak. The chimneys (low amplitude, vertically aligned features), indicated by black arrows, are also poorly visible. b: Proper illumination of the seismic image for inline no. 693 by conditioning the data using DSMF, showing the signal enhancement at places where the image was poor (indicated by ovals and arrows in Fig. 5a). (For interpretation of the references to colour in this figure legend, the reader is referred to the web version of this article.)

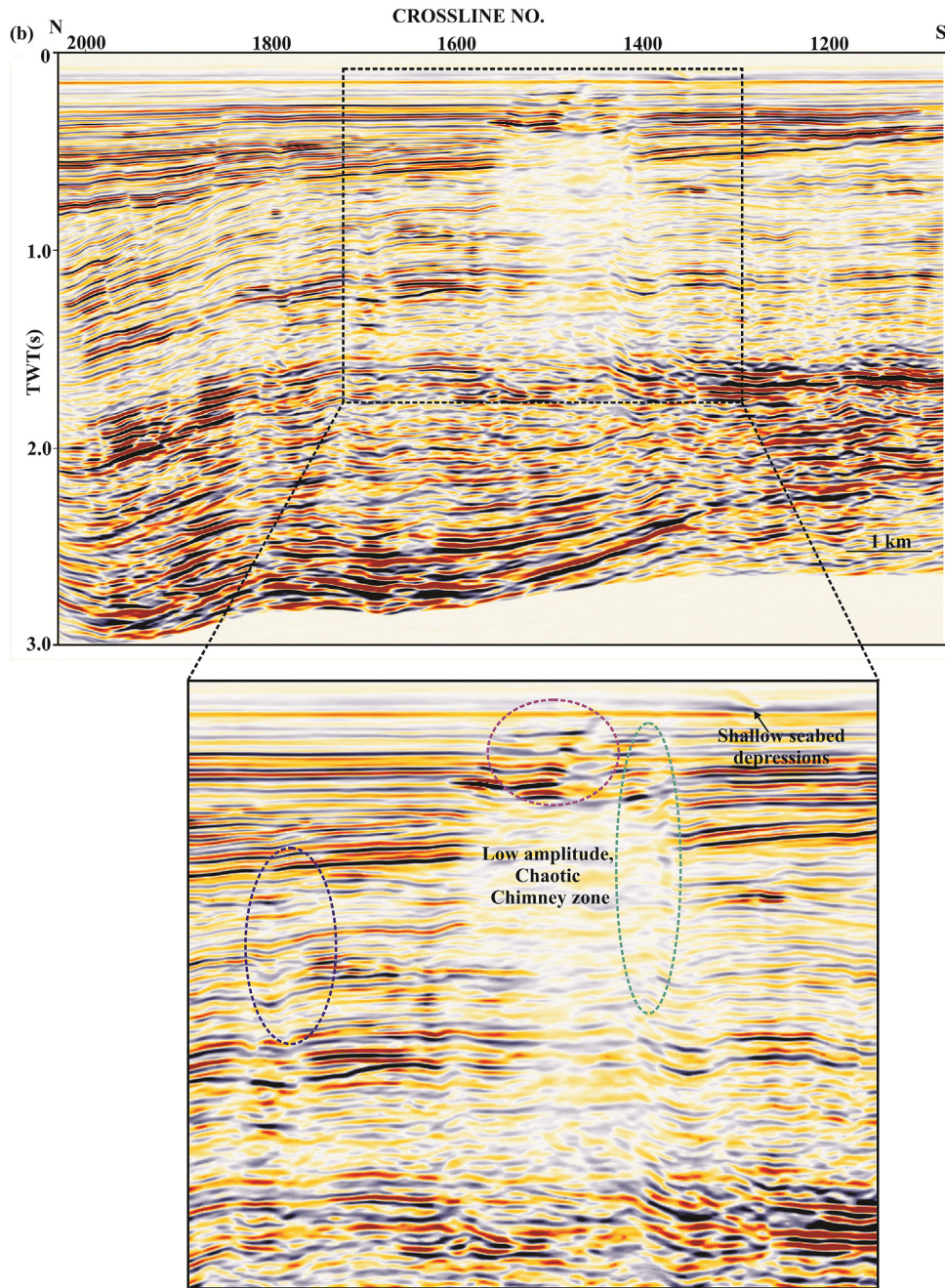


Fig. 5. (continued).

$$\text{var}(p_x) = \frac{1}{n-1} \sum_{\beta=-x_s}^{x_s} \sum_{\alpha=-y_s}^{y_s} \sum_{\tau=t_1}^{t_2} \left(p_x(x+\alpha, y+\beta, t+\tau) - \bar{p}_x \right)^2 \quad (4)$$

where, $\bar{p}_x = \left(\sum_{\beta=-x_s}^{x_s} \sum_{\alpha=-y_s}^{y_s} \sum_{\tau=t_1}^{t_2} p_x(x+\alpha, y+\beta, t+\tau) \right)$

t_1 and t_2 are the relative start and stop times, and n is the total number of samples in the sub-cube. x_s and y_s are the sub-cubes lateral step-out in x and y directions respectively. Equation (4) shows the dip variance in the x direction. Similarly, the dip variance in the y direction $\text{var}(p_y)$ can be calculated. The overall dip variance is then calculated by averaging the $\text{var}(p_x)$ and $\text{var}(p_y)$ as:

$$\overline{p_{\text{var}}} = \frac{\text{var}(p_x) + \text{var}(p_y)}{2} \quad (5)$$

4.2.4. Frequency wash-out

Higher frequency is attenuated more in the gas chimney because of scattering of the signal within the gas clouds. Thus, high frequency wash-out can be used as a good marker for the identification of gas chimneys.

4.2.5. Simple chimney attribute

The simple chimney attribute acts as a contributory tool for guiding other attributes (Connolly and Garcia, 2012). This is analyzed effectively with similarity attribute for testing low similar chaotic chimney zones.

All these attributes have been extracted from seismic data in the

Maari field of the Taranaki basin in three separate time windows: above, below and on the point of investigation. Most of the time windows used for attribute extraction have a length of 80 m, which is based on the fact that chimneys are vertical bodies with a certain dimension.

5. Methodology

Seismic chimneys are characterized by vertical disruption in the continuity of seismic reflectors and represented by low amplitude chaotic zones on seismic sections (Brouwer et al., 2008, 2011). However, some features such as the faults and mass transport deposits are also illuminated by low amplitudes and low similarity values (Brouwer et al., 2011). A combination of multiple attributes through a non-linear neural network provides an optimal approach for better interpreting these disrupted features from seismic data. (Heggland et al., 1999, 2000; Meldahl et al., 1999, 2001).

5.1. Seismic data conditioning

Noises such as the dispersion, scattering, diffractions etc. mask signals on seismic sections representing the subsurface. Thus, it has been routine to preprocess and optimally condition the seismic data before inferring meaningful geological interpretation. The workflow for conditioning the data is shown in Fig. 4. It begins with a process, called dip-steering (Tingdahl, 1999; Tingdahl et al., 2001; Tingdahl and de Groot, 2003; Qayyum et al., 2015; Jaglan et al., 2015) that uses local dip and azimuth of seismic events to track them locally with respect to the trace segments under investigation. The output of this process is known as the “dip-azimuth

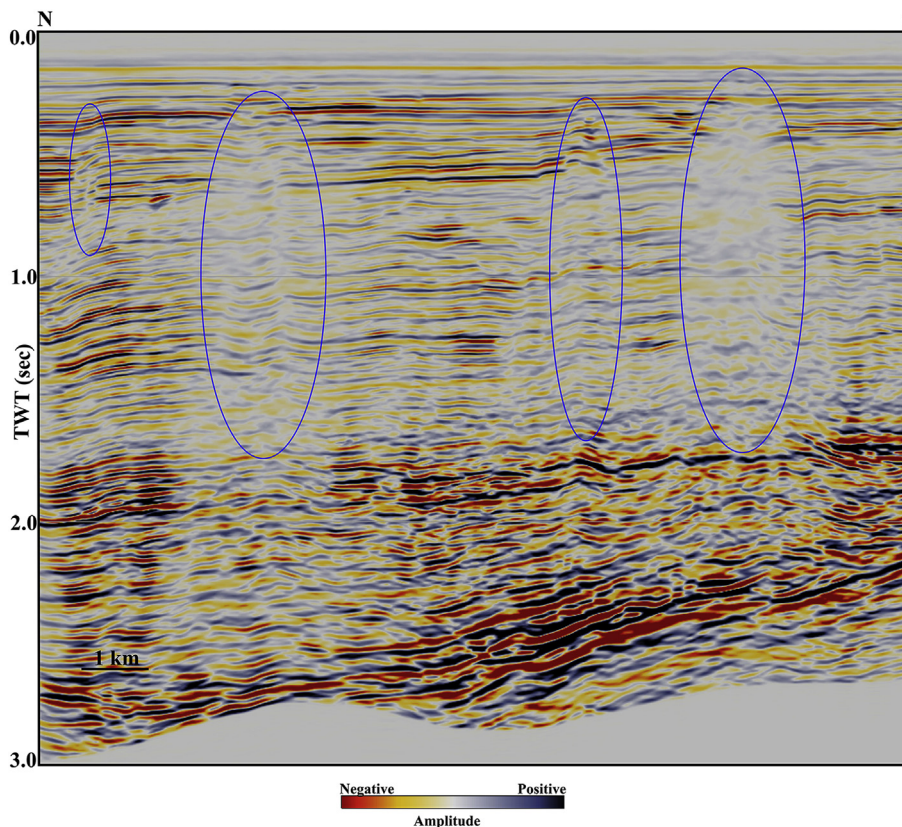


Fig. 6. DSMF seismic section for inline no. 793 from Maari 3D seismic volume. The section depicts chimney anomalies, marked by blue ovals. (For interpretation of the references to colour in this figure legend, the reader is referred to the web version of this article.)

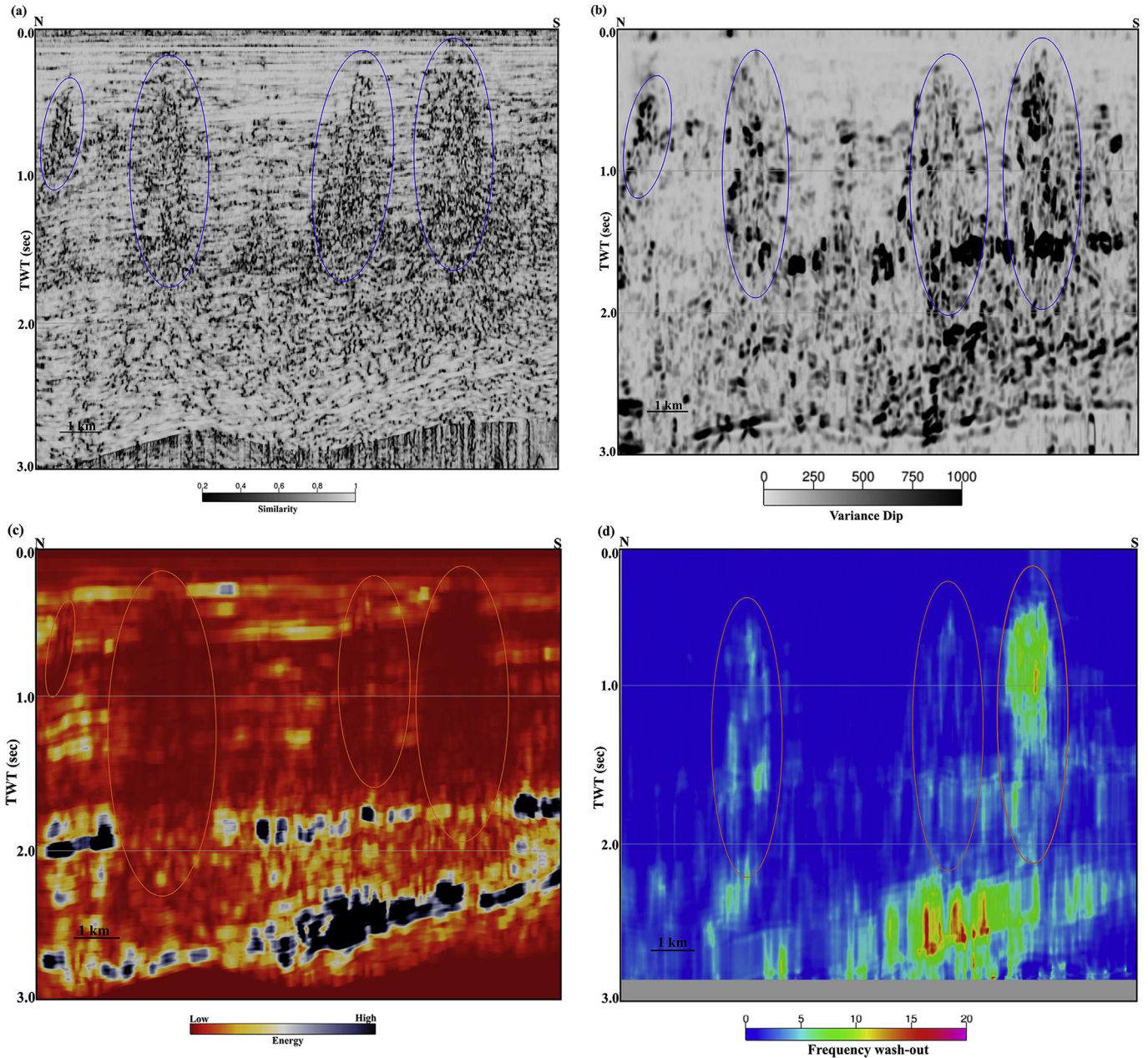


Fig. 7. a: Dip-steered similarity attribute in vertical section for inline no. 793 depicting the chimney anomalies marked by blue ovals associated with low similarity values. b: Variance dip attribute in vertical seismic section for inline no. 793 from Maari 3D seismic volume. The chimney zones (blue ovals) are associated with high variance dips. c: Energy attribute for inline no. 793. The chimney zones (orange ovals) are associated with low energy. d: Frequency wash-out attribute for inline no. 793. Note that chaotic chimney zones (red ovals) are associated with high frequency attenuation. (For interpretation of the references to colour in this figure legend, the reader is referred to the web version of this article.)

volume” or “steering cube”. A statistical filter, called the dip-steered median filter (DSMF), is applied to the seismic data volume (Fig. 5a) using the pre-processed steering cube, resulting into a smoothed seismic volume, known as the DSMF seismic volume (Fig. 5b). The DSMF seismic volume shows the continuity of seismic reflections and suppression of random noises (Jaglan et al., 2015; Qayyum et al., 2015), and is taken as input for the next operations.

5.2. Selection of input seismic attributes

Seismic attributes are used to comprehend information about objects from seismic data (Meldahl et al., 2001). It is essential to

have a prior knowledge on the geometrical characteristics such as the shape and orientation of the objects that we look for. This helps in selecting a set of seismic attributes that exhibit the best interpretation of gas chimneys, recognized as vertically aligned objects (Fig. 6). Seismic attributes such as the similarity (Fig. 7a), dip variance (Fig. 7b), energy (Fig. 7c) and frequency wash-out (Fig. 7d) are selected for studying the gas chimney. Other attributes such as the signal-to-noise ratio and two-way time are also taken into account. All these attributes are initially tested along few key seismic lines to demonstrate their ability in demarcating the chimneys more clearly. Once satisfactory result is achieved, all the attribute sets are chosen as input for the NN process.

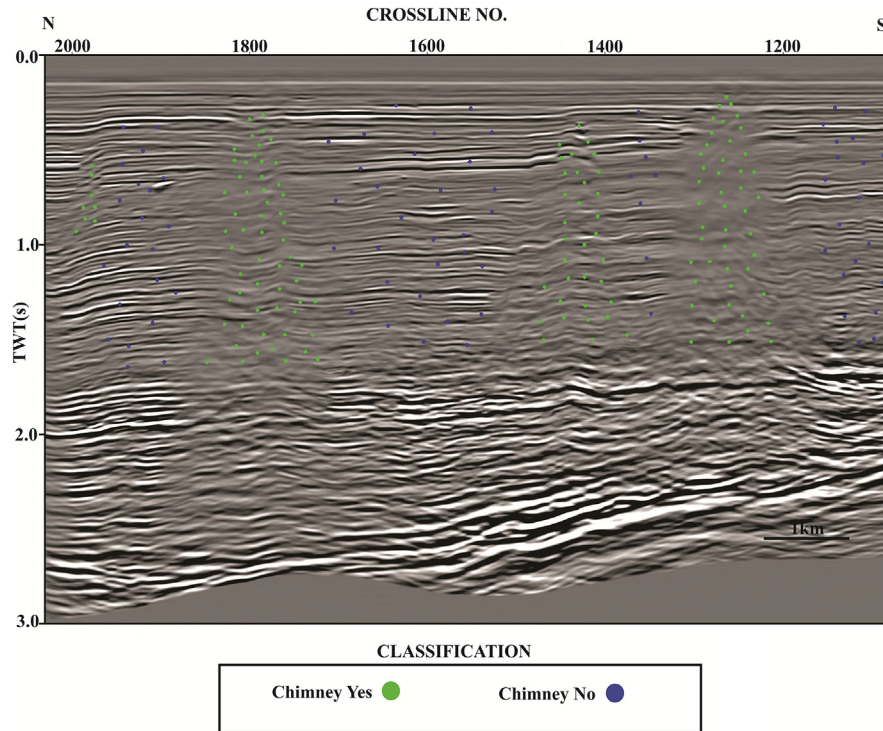


Fig. 8. Example locations of picksets for inline no. 793, which are classified into chimney-yes (green dots) and chimney-no (blue dots) groups. The MLP network learns through these examples. (For interpretation of the references to colour in this figure legend, the reader is referred to the web version of this article.)

5.3. Selection of training data

Example or pickset locations are provided to the NN to guide it how to discriminate the character (found in the input attribute sets) of chimney from non-chimney zones. Chimney picks (Fig. 8) are taken at the most obvious locations of vertical hydrocarbon migration pathways, characterized by low amplitude anomalies and chaotic zones. Non-chimney picks (Fig. 8) are taken at the locations without any migration pathways. Around 300 training locations have been selected in the seismic data volume.

5.4. Training of the NN

The NN learns from these examples, trains itself through the data and tries to establish a relationship between the input sets (seismic attributes) and the output (chimney-yes and chimney-no) (Fig. 9). The training is carried out iteratively and the weights of the connections are adjusted unless a minimum error between the predicted network result and the known output is reached. The training results are visualized on key seismic lines for quality check. Once satisfied, the NN is applied over the entire seismic volume to obtain the chimney probability volume. The volume contains values between 0 and 1, where 0 corresponds to the lowest probability of chimneys and 1 corresponds to the highest probability of chimney. The chimney volume is viewed by overlying it on seismic sections, formation tops and time slices.

5.5. Validation

The chimney validations are carried out as follows:

5.5.1. Geological validation

Geological knowledge from available information is important in carrying out this study. The tops of different geologic formations, as observed in the drilled well, are mapped over the seismic

volume. Seismic attributes and chimney probability cube are then examined for plausible geological features such as faults and their intersections over these formations with a view to ascertain the presence of gas seepage and accumulation (Gartrell et al., 2003;

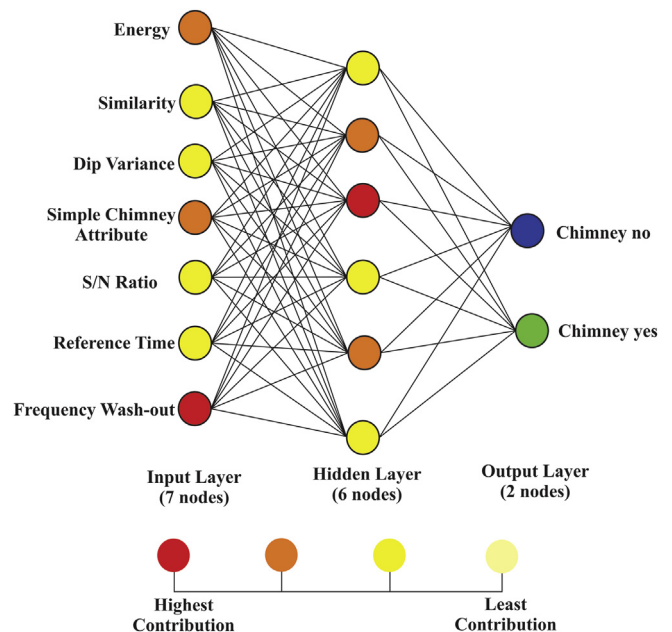









Fig. 9. The MLP network used for this study contains three different layers: input layer, hidden layer and output layer. Each layer consists of different nodes interconnected with each other as shown in the figure. The color scale red to pale yellow specifies the relative contribution or weights of each input node to the classification result. Red color provides much contribution in training for chimney. (For interpretation of the references to colour in this figure legend, the reader is referred to the web version of this article.)

Table 1

A sensitivity chart showing the relative contribution of all the attributes. Color codes are used to indicate maximum and minimum contributions of attributes used for neural training.

ATTRIBUTES	COLOR CODES	WEIGHTS
Similarity		52.5
Energy		70.4
Frequency wash-out		98.20
Simple Chimney Attribute		69.4
Dip Variance		42.4
Reference Time (TWT)		36.1
Signal/Noise (S/N)		27.4

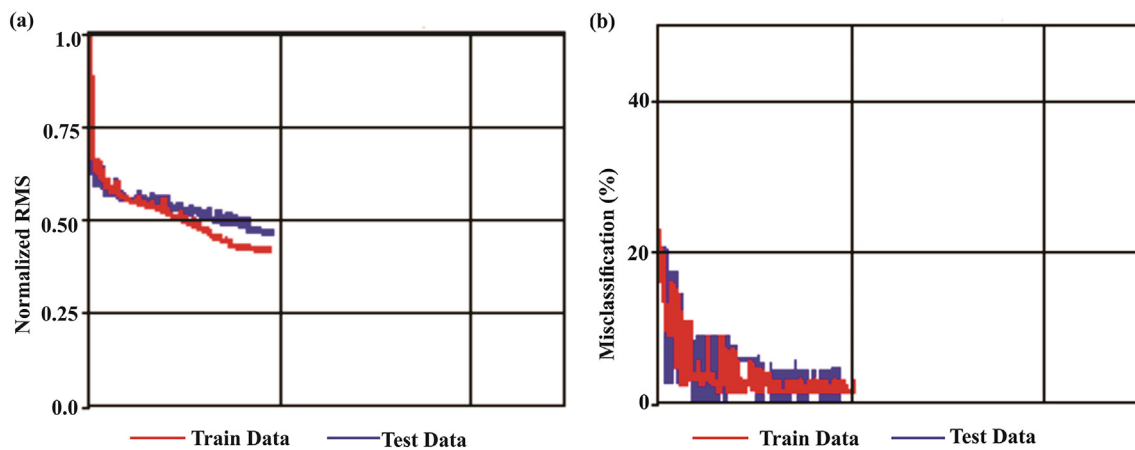
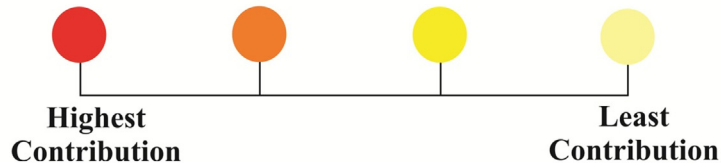


Fig. 10. a: Normalized RMS error between the observed and predicted attribute for the train (red) and test (blue) data sets. b: Misclassification percentage for training and testing phases. (For interpretation of the references to colour in this figure legend, the reader is referred to the web version of this article.)

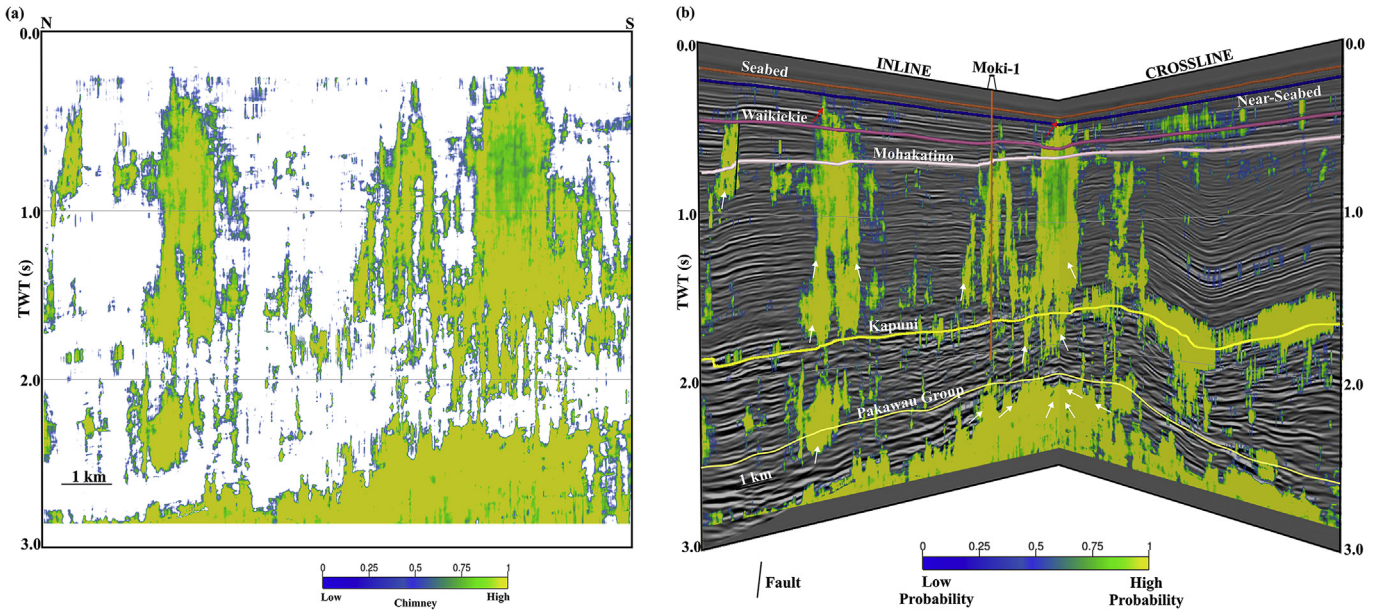


Fig. 11. a: The chimney probability output for inline no.793. High chimney probabilities are indicated by deep yellow color, whereas low probabilities are indicated by blue color. b: Chimney attribute volume overlain in the vertical seismic section for inline no. 793 and crossline no. 1253, showing the gas chimneys moving upwards from the source rock through the reservoirs (white arrows) to the seabed (red arrows). (For interpretation of the references to colour in this figure legend, the reader is referred to the web version of this article.)

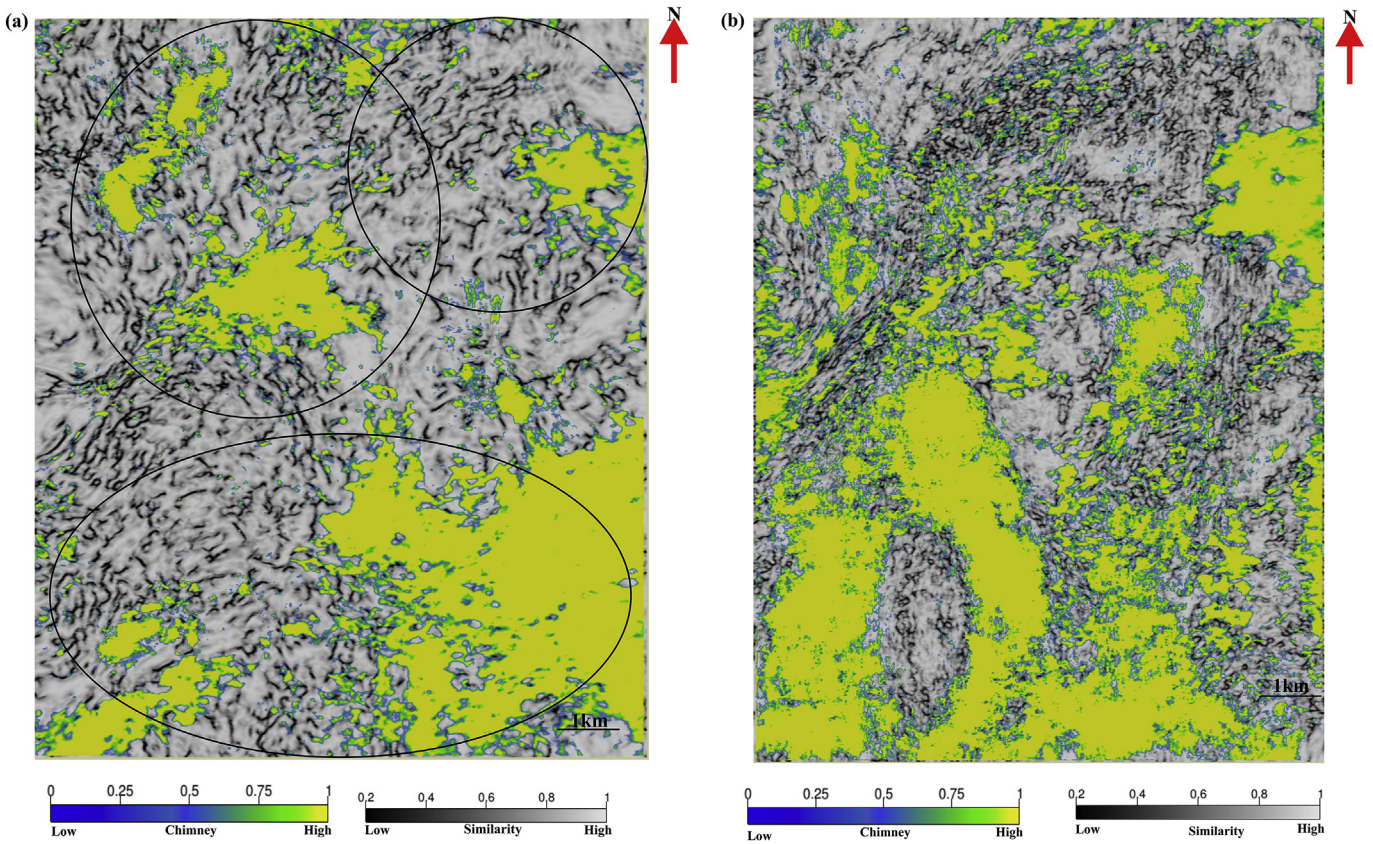


Fig. 12. a: Chimney and similarity attributes, co-rendered at 2500 m time slice that cuts the Pakawau Group. The presence of polygonal faults are clearly observed throughout the formation. The fault systems are associated with high gas chimneys (black ovals). b: Chimney and similarity attributes, co-rendered at 1660 m time slice that cuts the Kapuni Group.

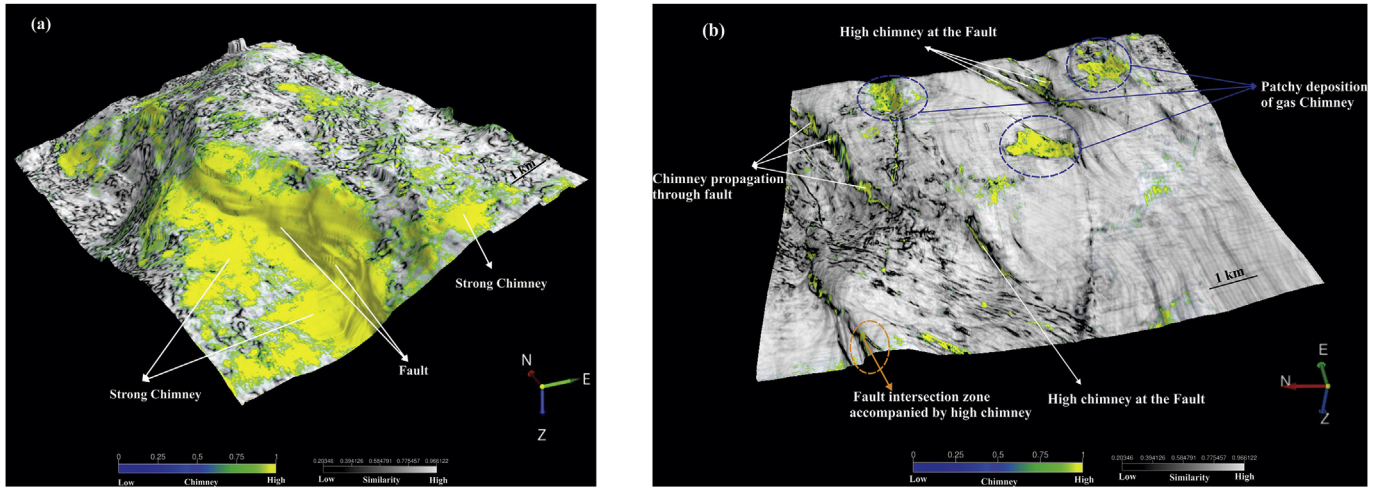


Fig. 13. a: Chimney and similarity attributes, co-rendered at horizon slice over the Kapuni Formation. Chimney effects (high probability) are observed along the fault zones (low similarity). High faulting activities along with several weak zones are observed within the formation. The weak zones act as conducive pathways for the gas to seep through them. Vertical exaggeration used for this visualization is 6.0. b: Chimney and similarity attributes, co-rendered at horizon slice over the Mohakatino Formation. Patchy distributions of gas chimneys are mostly observed towards NE and SE parts. Fault related chimneys are observed towards NE and NW part of the formation. Fault intersection zones accompanied by high chimney are highlighted (orange oval). Vertical exaggeration used for this visualization is 6.0. (For interpretation of the references to colour in this figure legend, the reader is referred to the web version of this article.)

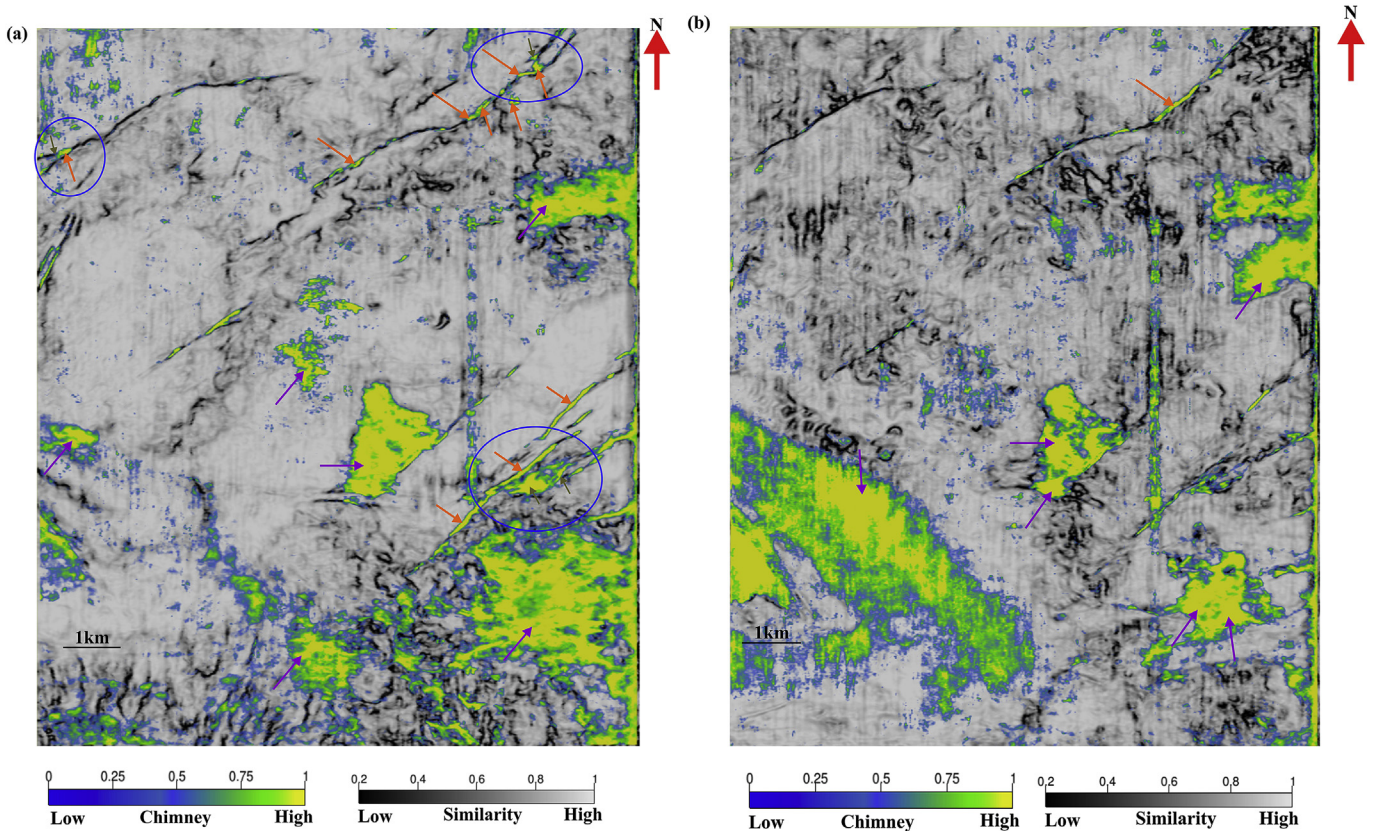


Fig. 14. a: Chimney and similarity attributes, co-rendered at 560 m time slice that cuts the Mohakatino Formation. Chimneys are distributed in patches (purple arrows). High probability chimneys (orange arrows) are observed along the faults. Blue ovals in the NE, NW and eastern parts highlighting the fault intersection (violet arrows) are characterized by high chimney effects. b: Chimney and similarity attributes, co-rendered at 440 m time slice that cuts the Waikiekie Formation. Gas chimneys (violet arrows) are observed in the central and NE parts of the formation. Faults, observed in the extreme northern part of the formation, are associated with high gas chimney (orange arrows). (For interpretation of the references to colour in this figure legend, the reader is referred to the web version of this article.)

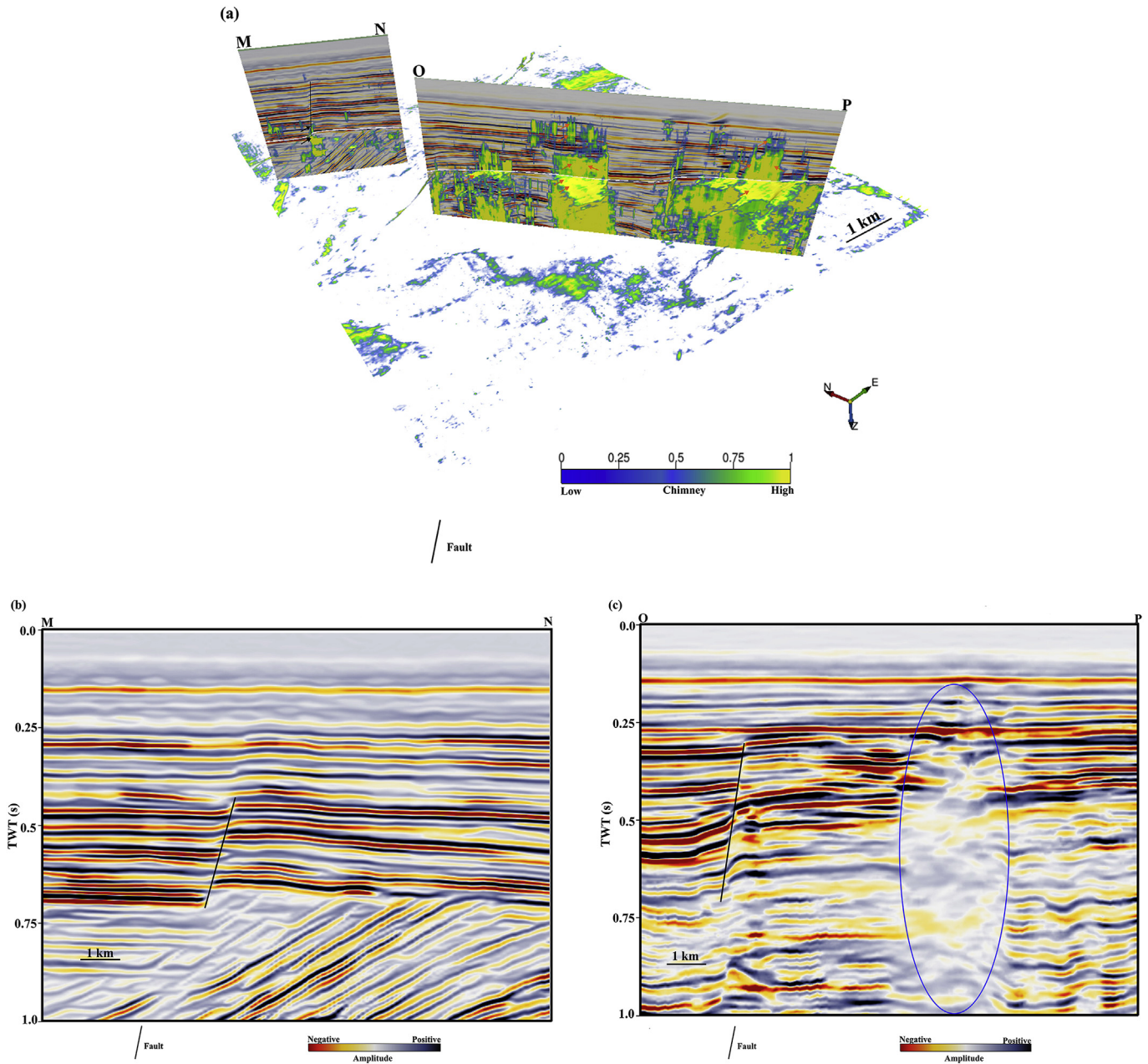


Fig. 15. a: Chimney attributes over the horizon slice of the Mohakatino Formation. Random lines MN and OP are drawn perpendicular to these chimney zones to show the correlation with the vertical seismic sections. Vertical migration pathways (orange arrows) show the gas chimneys along the line OP. Whereas, fault related chimneys are observed along the line MN. b: Random seismic section upto 1.0 s along MN showing the fault. c: Random seismic section upto 1.0 s along OP showing the fault and chimney zone (blue oval). (For interpretation of the references to colour in this figure legend, the reader is referred to the web version of this article.)

O'Brien et al., 2002; Ligtenberg, 2005).

5.5.2. Petrophysical validation

The petrophysical properties from the density (RHOB) and neutron porosity (NPHI) logs in the Moki-1 well (TEOL, 1984) have been looked into for correlation with different geologic formations. The response of the logs and gas shows encountered during drilling are analyzed to mark the gas related effects.

5.5.3. Soft sediment deformation anomalies

The effects of gas seepage, venting of oil or mobilized sediments through the seabed are observed in the form of some markers such as the pockmarks, mud diapirs and mud volcanoes (Løseth et al.,

2009). Observation of these features over the seismic data (sections, time slices, horizon slices) validates the presence of chimneys.

Once the network is tested and validated with several key elements, the 3D chimney cube is used for 2D and 3D displays. Such type of neural networks can also be used to identify other geologic features of interest such as the geologic faults, channels, salt bodies etc. from the seismic data.

6. Analysis and interpretation

The MLP network (Fig. 9) comprises of 15 fully connected nodes, 7, 6 and 2 nodes of which are associated with the input, hidden and

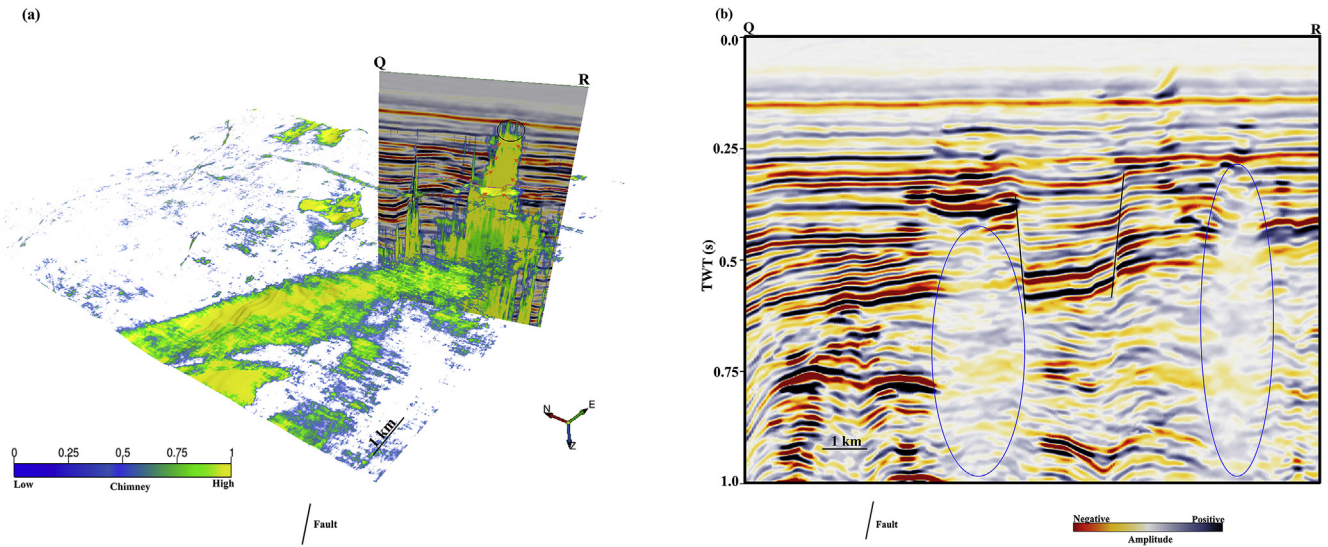


Fig. 16. a: Chimney attributes over the horizon slice of the Waikiekie Formation. Random line QR is drawn perpendicular to the chimney zone to show the correlation with the vertical seismic section. Vertical migration pathways (orange arrows) show the gas chimneys along the line QR. b: Random seismic section upto 1.0 s along QR showing the faults and chimney zones (blue oval). (For interpretation of the references to colour in this figure legend, the reader is referred to the web version of this article.)

output layers respectively. The network performs its operation by randomly splitting the data into train and test sets. 30% of the data is used for testing during which 48 input vectors are used. Whereas, 70% of data is used for training in which 106 input vectors are used. There is no invalid input vector in both cases. Iterative training and updating the connection weights overcome the problems related to local minima. The relative contribution of all input attributes for classifying chimneys is shown in Table 1. It is observed that frequency wash-out provides the highest contribution followed by energy, simple chimney attribute and similarity. We observe that after 8 iterations, the RMS error for both the trained and tested data attain the minimum value between 0.4 and 0.6 (Fig. 10a). A minimum misclassification (%) of 5.08–10.26% is obtained during the training and testing phases (Fig. 10b).

The chimney probability volume obtained from this neural training is interpreted using several visualization displays like vertical seismic sections, horizon and time slices and random lines. The chimney output is displayed in vertical seismic section (Fig. 11a) that exhibits the extent of active gas leakage from the source through the reservoirs. This observation is highlighted more when the chimney output is overlain on the seismic data and is viewed three dimensionally (Fig. 11b). The chimneys are originated from the source rock intervals of the Pakawau Group belonging to the Late Cretaceous period, charging into the Kapuni Group of the Paleocene to the Eocene period and propagating through the Miocene reservoirs all the way to the seabed. Co-rendering the chimney and similarity attributes at 2500 m time slice (Fig. 12a) that cuts the Pakawau Group shows the existence of gas accumulation. High probability chimneys are represented by deep yellow color and low probable chimneys are indicated by green to blue color. This formation is also associated with several polygonal fault systems which are observed close to the gas zones. Development of layer bound fault systems within this formation provides a pathway for the gas to be charged into the overlying Kapuni Group. Co-rendering the chimney and similarity attributes at 1660 m time slice (Fig. 12b) that cuts the Kapuni Group also reveals the presence of gas accumulation. Most of the gas deposits are concentrated along the faults, as are observed on the horizon slice over the Kapuni Formation (Fig. 13a). The horizon slice prepared by co-

rendering the chimney and similarity attributes over the Mohakatino Formation (Miocene reservoir) exhibits that gas chimneys are distributed in patches and more pronounced in the NE and SE parts of the region (Fig. 13b). The Mohakatino Formation is deformed and highly faulted, characterized by low similarity. However, zones within these faults are characterized by high chimney values. The fault zones in the extreme northern, NW and SE parts of the formation are associated with high chimney probability. Fault intersections are observed in the NW, and the zones within these intersections are characterized by high chimney values. These observations infer not only the faulting nature of the formation but also imply that these faults are associated with weak zones that act as conducive pathways for gas seepage. The time slice (Fig. 14a) at 560 m that cuts the Mohakatino Formation also honors these observations. Some of the faults in the extreme northern and NW part over this time slice intersect with each other, and higher chimneys are observed at these zones. Chimney patches with higher probability are observed over the NE and SE parts of the formation. Similar analysis is also carried over the time slice of 440 m that cuts the Waikiekie Formation, which exhibit patchy distribution of chimneys in the SW, SE and NE parts of the formation (Fig. 14b). Sharp signatures of faults, characterized by low similarity, are observed over this formation. The faults are also associated with high chimney patches. However, the faults observed in NW part of the formation do not show the signature of gas chimney, indicating that the faults are sealed in the NW part.

To understand more about the gas shows, as revealed by seismic attributes, we display seismic sections along random seismic lines, perpendicular to the trend of the chimney features over the horizon slice corresponding to the Mohakatino Formation (Fig. 15a). The random seismic section MN shows the fault related gas migration through the Mohakatino Formation of the Early Miocene. The random seismic section OP shows the vertical migration of gas through this formation, all the way to the seabed. The random seismic sections along MN and OP are shown in Fig. 15b and c respectively. Similar analysis is also carried over the Waikiekie Formation (Fig. 16a). The random seismic section QR over the Waikiekie Formation of the Late Miocene to Early Pliocene also exhibits gas migrations all the way to the seabed. The random

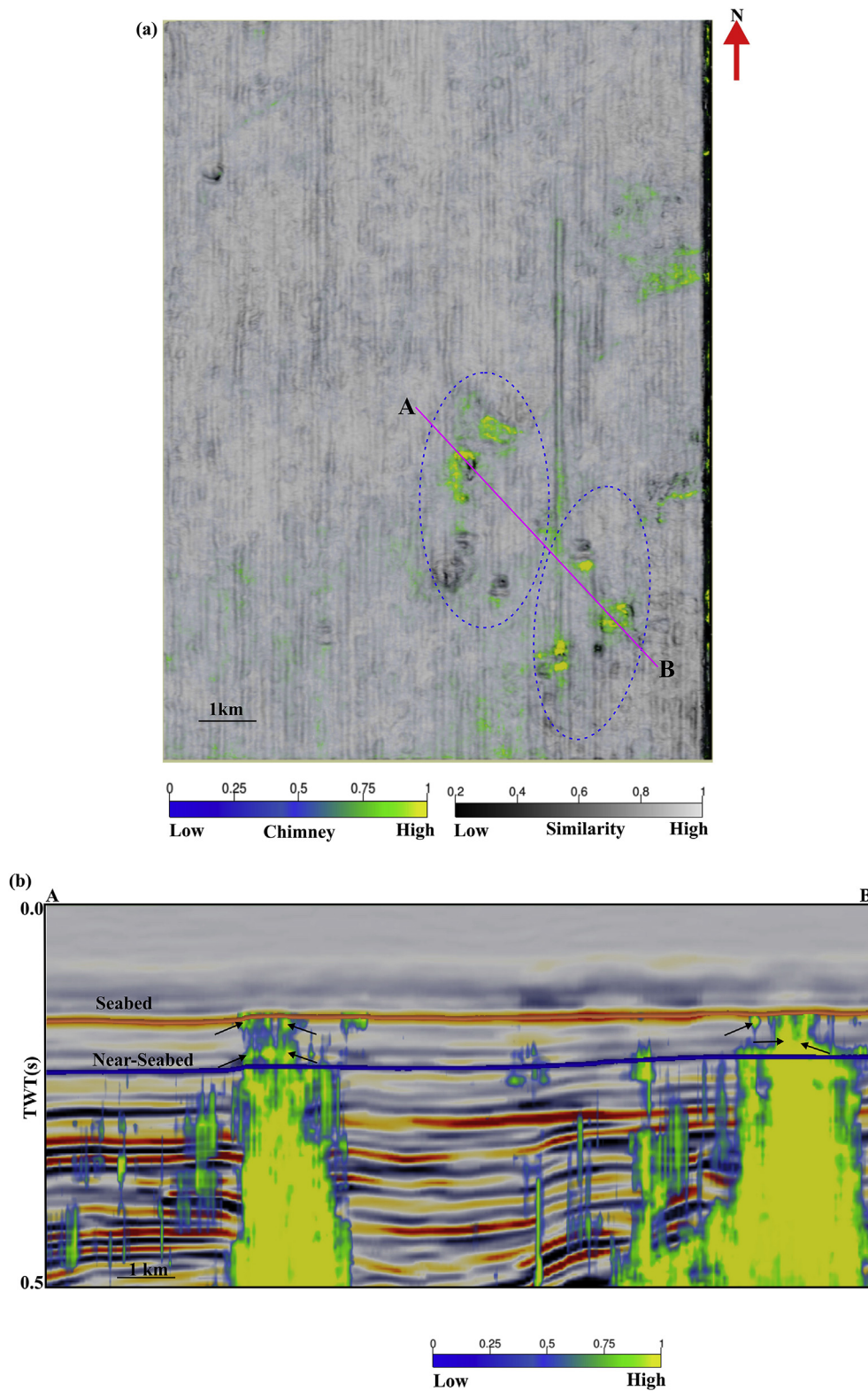


Fig. 17. a: Chimney and similarity attributes, co-rendered at 152 m time slice for the seabed. Pockmarks (circular morphology) are indicated by blue dotted ovals, which are associated with high chimney probability and reveals gas seepage through the seabed. To confirm this observation random line AB is drawn perpendicular to these pockmarks. b: Random seismic section upto 0.5 s along AB showing the chimney attribute. Vertical gas migrations (black arrows) are observed from the source to the seabed through the near-seabed. (For interpretation of the references to colour in this figure legend, the reader is referred to the web version of this article.)

seismic section along QR is shown in Fig. 16b. We display the time slice at 152 m over the seabed, overlain with the co-rendering of chimney and similarity attributes, with a view to observe the signature of gas migration (Fig. 17a). The pockmarks (circular appearance), observed over the seabed, are associated with low similarity and high chimney attributes. These features are nothing but the seafloor depressions caused by the escape of fluids and gases through them (Petersen et al., 2010). To observe the signature at depths, we look into the random seismic section along line AB passing through these circular features. The random seismic section (Fig. 17b) shows the gas escape from the shallow reservoirs all the way to the seabed.

Presence of gas has been established by drilling few wells at selected sites in the study region (TEOL, 1984). The location of Moki-1 well is shown in the 3D view of chimney overlain with seismic sections (Fig. 11b), where gas shows are encountered at depths ranging from 1100 m below kelly bush (mbkb) to 2600 mbkb (Fig. 18). These are also indicated by the decrease in observed density and porosity logs. The well was drilled upto a

depth of 2620 mbkb, and we don't have any information below this depth. We also don't have any well information above 650 mbkb. Our findings based on seismic attribute studies are corroborated with the drilling results, and provides further information on the prospective zones of gas occurrences in the study region.

The entire study has been summarized in Fig. 19, which shows that the gas clouds originating from the Pakawau Group (source rock) of the Late Cretaceous age, propagate through the overlying Kapuni Group of the Eocene and Wai-iti Group (Mohakatino and Waikiekie Formations) of the Miocene reservoirs to the seabed. Frequency attenuation and signal deterioration between the deep and shallow reservoirs reveal that gas chimneys extend through the formation to the seabed, which is indicated by pockmarks or wipe-out zones. Thus, the present workflow helps in understanding the petroleum system of a region, and provides a measure in mitigating hazards, caused by overpressure due to the presence of gas.

We have used the MLP network to classify chimney and non-chimney zones from seismic data. This is a supervised learning process, where the network learns by example sets (i.e. chimney

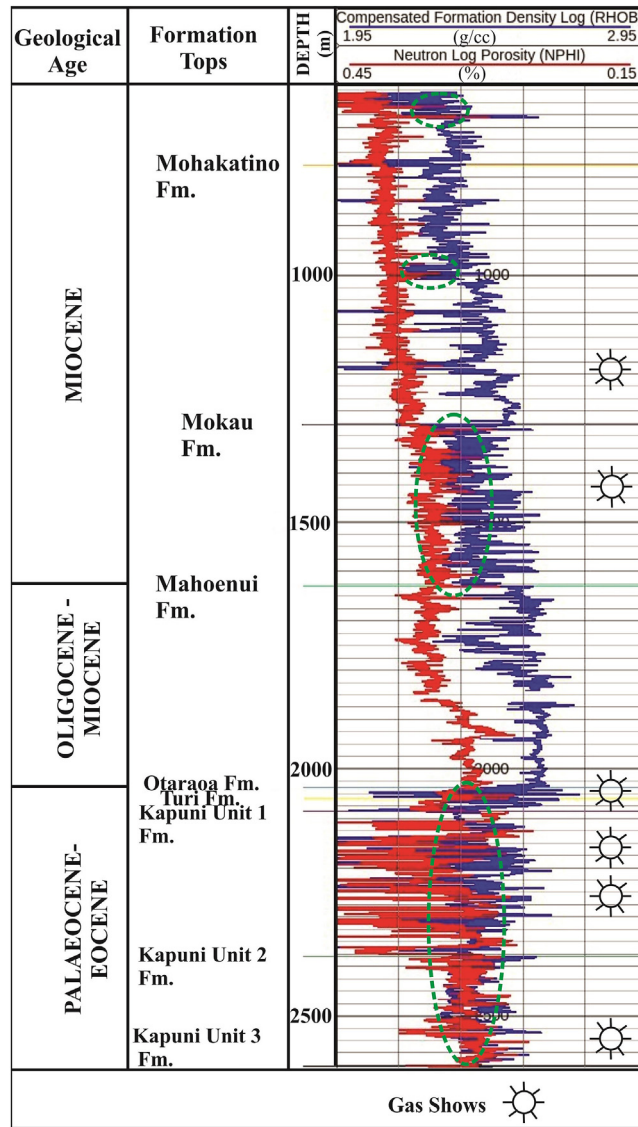


Fig. 18. The density and neutron porosity logs at Well Moki-1 passing through the study area. The decreasing trend of both logs (green dotted ovals) indicate the depth interval of gas shows, which were encountered in the well at depths, marked by circular symbols. (For interpretation of the references to colour in this figure legend, the reader is referred to the web version of this article.)

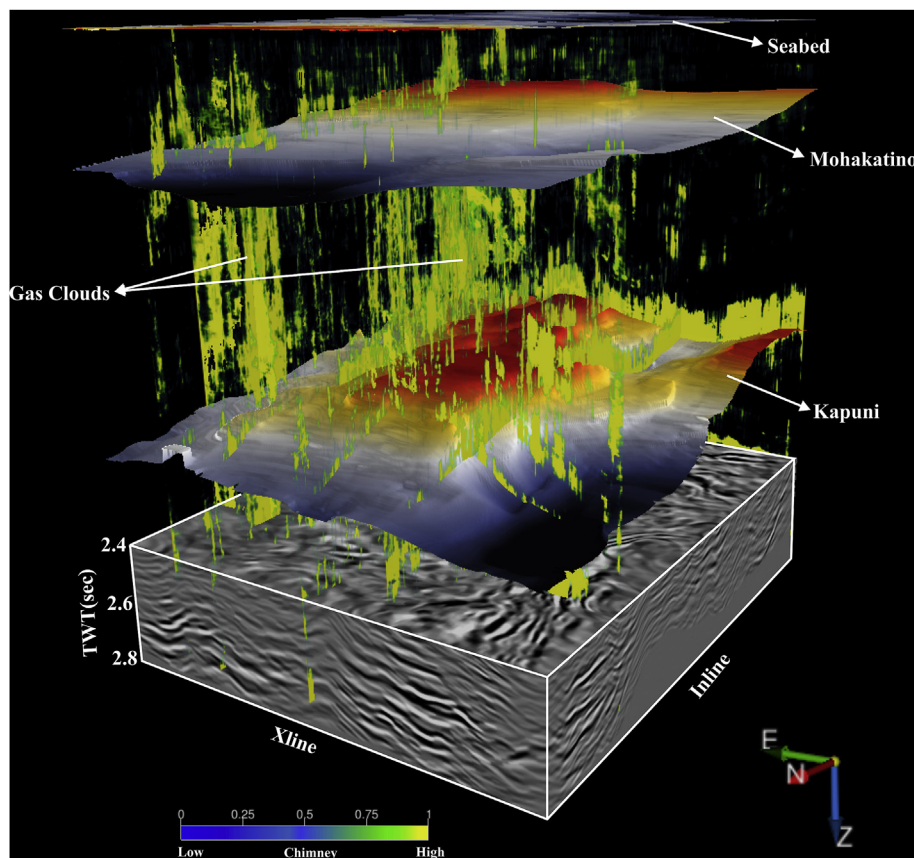


Fig. 19. 3D volumetric visualization of gas clouds or chimney showing its rise from the thermally mature source rock, propagating through the Eocene (Kapuni Formation) and Miocene (Mohakatino Formation) reservoirs all the way to the seabed.

sets in our case) and uses a classification scheme for identifying features of interest. The advantages of using ANN through MLP is that the technique uses the interpreter's ability, insight and knowledge to prepare example sets and allows the network to learn by these examples. However, if we tend to perform a pattern analysis (i.e. use of NN to cluster the available data), then it is an unsupervised learning technique that may not solve the problem.

7. Conclusions

We have developed a new workflow based on neural network for the computation of new attribute(s) from a set of other attributes, which has been used in interpreting seismic data for discriminating geologic features from gas chimneys. The application of the approach to time migrated 3D seismic data in Maari field of the highly structured and deformed Taranaki basin has delineated gas zone that has been validated from the well data. The main conclusion from this study is the delineation of gas clouds that has originated from the Late Cretaceous source rocks followed by migration into the Eocene and Miocene sandstone reservoirs. The study also shows that gas has seeped through the overlying Pliocene to recent formations, the imprints of which are observed as pockmarks on the seabed. This workflow can also be used for interpreting plausible geological features such as the faults, mud diapirs, mud volcanoes, salt bodies, slum deposits, debris flows etc. from seismic data. The technique can be extended in characterizing reservoir properties such as the porosity, permeability, saturation etc.

Acknowledgement

We thank the Director, CSIR-NGRI for according permission to carry out this work. Thanks are due to dGB Earth Science™ for providing academic license of OpendTect™ (v5.0.11) software. New Zealand Petroleum & Minerals, Ministry of Business, Innovation & Employment, New Zealand Government are highly acknowledged for providing seismic and well data sets. We also thank two anonymous reviewers and the Editor for providing valuable suggestions and useful comments. Mr. Jitender Kumar is thanked for his support at various stages of the work. This is a contribution to GEOSCAPE project of NGRI under the 12th five year scientific program of CSIR.

References

- Al-Dossary, S., Marfurt, K.J., 2006. 3-D volumetric multi-spectral estimates of reflector curvature and rotation. *Geophysics* 71, 41–51.
- Alotaibi, Mohammed Dhaifallah M., 2015. Seismic Structural Investigation and Reservoir Characterization of the Moki Formation in Maari Field, Taranaki Basin, New Zealand. Master Theses, paper 7459.
- Aminzadeh, F., Connolly, D., Heggland, R., de Groot, P.F.M., 2002. Geo-hazard detection and other application of chimney cubes. *Lead. Edge* 21, 681–685.
- An, P., Moon, W.M., 1993. Reservoir characterization using feed-forward neural networks. *SEG Tech. Program Expand. Abstr.* 258–262.
- Atakulreka, A., Sutivong, D., 2007. Avoiding local minima in feedforward neural networks by simultaneous learning. In *Australasian Joint Conference on Artificial Intelligence*, 100–109.
- Bahorich, M., Farmer, S., 1995. 3-D seismic discontinuity for faults and stratigraphic features: the coherence cube. *Lead. edge* 14, 1053–1058.
- Berndt, C., Bunz, S., Mienert, J., 2003. Polygonal fault systems on the Mid-Norwegian margin: a long-term source for fluid flow. In: Rensbergen, P.V., Hills, R., Maltman, A., Morley, C. (Eds.), *Origin, Processes, and Effects of Subsurface*

- Sediment Mobilization on Reservoir to Regional Scale. Geological Society of London (Special Publication).
- Brouwer, F.G.C., Welsh, A., Connolly, D.L., Selva, C., Curia, D., Huck, A., 2008. High Frequencies Attenuation and Low Frequency Shadows in Seismic Data Caused by Gas Chimneys, Onshore Ecuador. In 70th EAGE Conference and Exhibition incorporating SPE EUROPEC 2008.
- Brouwer, F., Tingdahl, K., Connolly, D., Dec. 2011. A Guide to the Practical Use of Neural Networks. 31st Annual Gulf Coast Section SEPM Foundation Bob F. Perkins Research Conference, Houston, Texas, 4–7.
- Chen, G., Matteucci, G., Fahmi, B., Finn, Ch, 2008. Spectral-decomposition response to reservoir fluids from a deepwater West Africa reservoir. *Geophysics* 73, 23–30.
- Chopra, S., Marfurt, K.J., 2007. Seismic Attributes for Prospect Identification and Reservoir Characterization. SEG, Tulsa.
- Connolly, D., Garcia, R., 2012. GEOLOGY & GEOPHYSICS-tracking Hydrocarbon Seepage in Argentina's Neuquén Basin. *World Oil*, pp. 101–104.
- de Groot, P.F.M., 1995. Seismic Reservoir Characterisation Employing Factual and Simulating Wells. Delft University Press, ISBN 90-407-1163-1.
- de Groot, P.F.M., 1999. Seismic reservoir characterisation using artificial neural networks. In: 19th Mintrop Seminar, pp. 16–18.
- de Groot, P.F.M., Ligtenberg, H., Oldenziel, T., Connolly, D., Meldahl, P., 2004. Examples of Multi-attribute, Neural Network-based Seismic Object Detection, vol. 29. Geological Society, London, Memoirs, pp. 335–338.
- Dunbar, T., Hofland, G., Davis, B., 1998. 3D Depth Imaging Through a Gas Cloud Using a Phased Velocity Modelling Approach. In: 60th EAGE Conference and Exhibition, Session: 01–44.
- Engelhardt, T., Randazzo, S., Bertagne, A., Cafarelli, B., 2001. Interpretation of four-component seismic data in a gas cloud area of the central Gulf of Mexico. *Lead. Edge* 20, 400–407.
- Farfour, M., Yoon, W.J., Kim, J., 2015. Seismic attributes and acoustic impedance inversion in interpretation of complex hydrocarbon reservoirs. *J. Appl. Geophys.* 114, 68–80.
- Gartrell, A., Zhang, Y., Lisk, M., Dewhurst, D., 2003. Enhanced hydrocarbon leakage at fault intersections: an example from the Timor Sea, Northwest shelf, Australia. *J. Geochem. Explor.* 78, 361–365.
- Hardage, B.A., Carr, D.L., Lancaster, D.E., Simons, J.L., Hamilton, D.S., Elphick, R.Y., Oliver, K.L., Johns, R.A., 1996. 3D seismic imaging and seismic attribute analysis of genetic sequences situated in low accommodation conditions. *Geophysics* 61, 1351–1362.
- Hart, A., 2001. Taranaki basin yielding large oil and gas discoveries. *Oil Gas J.* 99, 38–44.
- Heggland, R., 1997. Detection of gas migration from a deep source by the use of exploration 3D seismic data. *Mar. Geol.* 137, 41–47.
- Heggland, R., Meldahl, P., Bril, B., de Groot, P.F.M., 1999. The chimney cube, an example of semi-automated detection of seismic objects by directive attributes and neural networks: part II; interpretation. SEG 69th Annual Meeting Houston. *Expand. Abstr.* 1, 935–937.
- Heggland, R., Meldahl, P., de Groot, P.F.M., Aminzadeh, F., February 2000. Chimneys in the Gulf of Mexico. *The American Oil and Gas Reporter*, pp. 78–83.
- Heggland, R., 2004. Definition of geohazards in exploration 3-D seismic data using attributes and neural-network analysis. *AAPG Bull.* 88, 857–868.
- Higgs, K.E., King, P.R., Raine, J.I., Sykes, R., Browne, G.H., Crouch, E.M., Baur, J.R., 2012. Sequence stratigraphy and controls on reservoir sandstone distribution in an Eocene marginal marine-coastal plain fairway, Taranaki Basin, New Zealand. *Mar. Pet. Geol.* 32, 110–137.
- Ilg, B.R., Hemmings-Sykes, S., Nicol, A., Baur, J., Fohrmann, M., Funnell, R., Milner, M., 2012. Normal faults and gas migration in an active plate boundary, southern Taranaki Basin, offshore New Zealand. *AAPG Bull.* 96, 1733–1756.
- Jaglan, H., Qayyum, F., Huck, H., 2015. Unconventional seismic attributes for fracture characterization: first Break, 33, 101–109.
- Kamp, P.J.J., Vonk, A.J., Bland, K.J., Hansen, R.J., Hendy, A.J., McIntyre, A.P., Ngatai, M., Cartwright, S.J., Hayton, S., Nelson, C.S., 2004. Neogene stratigraphic architecture and tectonic evolution of Wanganui, King Country and eastern Taranaki basins, New Zealand. *N. Z. J. Geol. Geophys.* 47, 625–644.
- King, P.R., Thrasher, G.P., 1996. Cretaceous-cenozoic Geology and Petroleum Systems of the Taranaki Basin, New Zealand. Institute of Geological and Nuclear Sciences, Lower Hutt (N.Z.). Monograph 13.
- King, P.R., Naish, T.R., Browne, G.H., Field, B.D., Edbrooke, S.W., 1999. Cretaceous to Recent Sedimentary Patterns in New Zealand. Folio Series 1. Institute of Geological and Nuclear Sciences, Lower Hutt.
- King, P.R., 2000. Tectonic reconstructions of New Zealand 40Ma to the present. *N. Z. J. Geol. Geophys.* 43, 611–638.
- Ligtenberg, J.H., Wansink, A.G., 2001. Neural network prediction of permeability in the El Garia Formation, Ashtart oilfield, offshore Tunisia. *J. Pet. Geol.* 24, 389–404.
- Ligtenberg, J.H., 2003. Unravelling the petroleum system by enhancing fluid migration paths in seismic data using a neural network based pattern recognition technique. *Geofluids* 4, 255–261.
- Ligtenberg, J.H., 2005. Detection of fluid migration pathways in seismic data: implications for fault seal analysis. *Basin Res.* 17, 141–153.
- Løseth, H., Gading, M., Wensaas, L., 2009. Hydrocarbon leakage interpreted on seismic data. *Mar. Pet. Geol.* 26, 1304–1319.
- Marfurt, K.J., Kirilin, R.L., Farmer, S.L., Bahorich, M.S., 1998. 3-D seismic attributes using a semblance-based coherency algorithm. *Geophysics* 63, 1150–1165.
- Marfurt, K.J., Sudhaker, V., Gersztenkorn, A., Crawford, K.D., Nissen, S.E., 1999. Coherency calculations in the presence of structural dip. *Geophysics* 64, 104–111.
- McCulloch, W.S., Pitts, W., 1943. A logical calculus of the ideas immanent in nervous activity. *Bull. Math. Biophys.* 54, 115–133.
- Meldahl, P., Heggland, R., Bril, B., de Groot, P., 1999. The chimney cube, an example of semi-automated detection of seismic objects by directive attributes and neural networks: Part I; methodology. In Annual Meeting, SEG Houston. *Expand. Abstr.* 1, 931–934.
- Meldahl, P., Heggland, R., Bril, B., de Groot, P., 2001. Identifying fault and gas chimneys using multi-attributes and neural networks. *Lead. Edge* 20, 474–482.
- Mohaghegh, S., Arefi, R., Ameri, S., Aminiand, K., Nutter, R., 1996. Petroleum reservoir characterization with the aid of artificial neural networks. *J. Pet. Sci. Eng.* 16, 263–274.
- O'Brien, M.J., Whitmore, N.D., Brandsberg-Dahl, S., Murphy, G.E., 1999. Multicomponent modeling of the Valhall field. In: 61st Conf. European Assoc. of Geoscientists and Engineers, Helsinki, Finland.
- O'Brien, G.W., Cowley, R., Quaife, P., Morse, M., 2002. Characterizing hydrocarbon migration and fault-seal integrity in Australia's Timor Sea via multiple, integrated remote-sensing technologies. Surface exploration case histories: applications of geochemistry, magnetics and remote sensing. *AAPG Stud. Geol.* 48, 393–413.
- Palmer, J.A., Andrews, P.B., 1993. Cretaceous-Tertiary sedimentation and implied tectonic controls on the structural evolution of Taranaki Basin. In: Balance, P.F. (Ed.), *South Pacific Sedimentary Basin of the World*, vol. 2. Elsevier, Amsterdam, pp. 309–328.
- Petersen, C.J., Bunz, S., Hustoft, S., Mienert, J., Klaeschen, D., 2010. High-resolution P-Cable 3D seismic imaging of gas chimney structures in gas hydrate sediments of an Arctic sediment drift. *Mar. Pet. Geol.* 27, 1981–1994.
- Qayyum, F., Catuneanu, O., Bouanga, C.E., 2015. Sequence stratigraphy of a mixed siliciclastic-carbonate setting, Scotian Shelf, Canada: Interpretation. SEG 3, SN21–SN37.
- Reilly, C., Nicol, A., Walsh, J.J., Seebeck, H., 2015. Evolution of faulting and plate boundary deformation in the Southern Taranaki Basin, New Zealand. *Tectonophysics* 651, 1–18.
- Roberts, A., 2001. Curvature attributes and their application to 3 D interpreted horizons. *First Break* 19, 85–100.
- Rosenblatt, F., 1962. Principles of Neurodynamics: Perceptrons and the Theory of Brain Mechanism. Spartan Books, 616 pp.
- Schuelke, J.S., Quirein, J.A., Sag, J.F., Altany, D.A., Hunt, P.E., 1997. Reservoir Architecture and Porosity Distribution, Pegasus Field, West Texas - an Integrated Sequence Stratigraphic-seismic Attribute Study Using Neural Networks. SEG Technical Program Expanded Abstracts, pp. 668–671.
- Tingdahl, K.M., 1999. Improving Seismic Detectability Using Intrinsic Directionality. Technical Report. Earth Sciences Center, Goteborg University, p. B194.
- Tingdahl, K.M., Bril, A.H., de Groot, P., 2001. Improving seismic chimney detection using directional attributes. *J. Pet. Sci. Eng.* 29, 205–211.
- Tingdahl, K.M., 2003. Improving seismic chimney detection using directional attributes. In: *Developments in Petroleum Science*, vol. 51. Elsevier Science Publishers, Amsterdam, pp. 157–173.
- Tingdahl, K.M., de Groot, P.E.M., 2003. Post-stack dip and azimuth processing. *J. Seism. Explor.* 12, 113–126.
- Tingdahl, K.M., de Rooij, M., 2005. Semi-automatic detection of faults in 3D seismic data. *Geophys. Prospect.* 53, 533–542.
- TEOL (Tricentrol Exploration Overseas Ltd, 1984. Well Completion Report Moki-1 PPL 38114. Ministry of Economic Development New Zealand. Unpublished Petroleum Report Series PR987.
- Van der Baan, M., Jutten, C., 2000. Neural networks in geophysical applications. *Geophysics* 65, 1032–1047.
- Westbrook, G.K., Exley, R., Minshull, T., Nouze, H., Gailler, A., Jose, T., Ker, S., Plaza, A., 2008. High-resolution 3D Seismic Investigations of Hydrate-bearing Fluid-escape Chimneys in the Nyegga Region of the Voring Plateau, Norway. In: *Proceedings of the 6th International Conference on Gas Hydrates, Vancouver, British Columbia, July 6–10*, pp.8.
- Wong, P.M., Jian, F.X., Taggart, I.J., 1995. A critical comparison of neural networks and discriminant analysis in lithofacies, porosity and permeability predictions. *J. Pet. Geol.* 18, 191–206.
- Wooltorton, T., 2015. Shallow hazard and gas escape systems modelling from 3D seismic. In: 2015 SEG Annual Meeting. Society of Exploration Geophysicists, pp. 1673–1676.